Chapter 13
Novel Neutron Imaging Techniques for Cultural Heritage Objects

C. Andreani, G. Gorini, and T. Materna

Abstract The use of neutrons for cultural heritage (CH) research is illustrated with special reference to neutron tomography (NT) methods, providing three-dimensional (3D) images of neutron attenuation, and the analysis techniques known as prompt gamma-ray activation analysis (PGAA) and neutron resonance capture analysis (NRCA), providing the elemental composition of an object. PGAA and NRCA are well-established nondestructive methods for bulk analysis of CH objects, with sensitivities that can reach the parts-per-million range. By improving the spatial resolution of PGAA and NRCA it will be possible to measure the composition of small parts inside a large object or even to provide a full 3D map of the elemental composition of an artifact. The imaging techniques under development are called prompt gamma-ray activation imaging (PGAI), neutron resonance capture imaging (NRCI) and neutron resonance transmission (NRT) tomography. The NRCA experience at the GELINA neutron source is the starting point for the development of NRCI/NRT now taking place at the 100 times more powerful ISIS pulsed neutron source.

PGAI, NRCI, and NRT are unlikely to achieve the spatial resolution obtained by conventional NT. It is the combined use of these new imaging techniques with neutron and X-ray tomographies that is proposed here as the way forward in neutron imaging. There are parallel developments in the use of Bragg edges to improve the elemental sensitivity of NT (dichromatic tomography). Another foreseen development is 3D phase imaging (neutron diffraction imaging, NDI), which can essentially be undertaken using existing diffraction instruments. The ongoing developments are promising and suggest that neutron-based techniques will provide the basis for integrated analysis protocols leading to important advances in the scientific characterization of the materials that constitute a CH object.

C. Andreani (✉)
University of Milano-Bicocca, Department of Materials Science, Via Roberto Cozzi 53, 20125 Milano, Italy

I.S. Anderson et al. (eds.), *Neutron Imaging and Applications*,
Neutron Scattering Applications and Techniques, DOI 10.1007/978-0-387-78693-3_13,

Keywords X-ray and neutron scattering · Neutron diffraction · Neutron imaging · Ancient Roman marbles · Textures · Experimental methods of materials testing and analysis

13.1 Imaging, Neutrons, and Cultural Heritage

The use of X-ray and neutron facilities for cultural heritage (CH) research is rapidly growing [1, 2]. Detailed three-dimensional (3D) maps of neutron and X-ray attenuation in CH objects are produced by the tomographic methods described earlier in this book. X-ray and neutron facilities also provide a number of nondestructive analytical techniques that are used in the CH field. X-ray fluorescence (XRF) is a well-known example, in particular because of the widespread use of portable XRF devices, a clear advantage for analysis of valuable objects at (or close to) museums. More generally, the application of nuclear-based techniques to CH research has expanded in recent years as laboratories with small ion accelerators have been installed close to museums, facilitating the study of CH objects by particle-induced X-ray and gamma-ray emission (PIXE and PIGE) and Rutherford backscattering [3].

With XRF and PIXE, imaging is possible down to micrometer resolution; but because both techniques are based on the detection of low-energy X-rays, only information on the surface of an object is retrieved. Bulk analysis techniques are alternatively available (see below) but do not offer a spatial resolution adequate for measuring the composition of small parts inside a large object well. Ideally, one would like to combine the spatial resolution of tomographic methods with the power of nondestructive analytical techniques to provide a 3D map of the elemental composition of a large object. Can neutrons be used for such a challenging task? The question is addressed in this chapter by first reviewing some general features of neutron (and X-ray) techniques as relevant for CH studies.

X-rays and neutrons conveniently complement each other in CH research. This is because CH objects can be made from diverse materials sampling the Mendeleev table at both low and high atomic numbers, making the attenuation of X-rays and neutrons very different. X-rays have a lower penetration depth at high atomic numbers. Thus X-ray radiography (XR) is suitable for probing the interior of objects made from wood or bone, but it has problems with bulky metals such as gold, silver, and lead, which are nearly opaque to X-rays. On the other hand, neutron radiography (NR) can probe metal artifacts (e.g., copper, tin, iron, bronze, lead) but does not penetrate thick layers of organic materials because of strong neutron beam attenuation by hydrogen. An introduction to NR and its applications can be found elsewhere in this book.

Neutron tomography (NT) is performed by taking a large set of radiographs of an object at different orientations and reconstructing all data offline in a virtual 3D image. For further details, see Chapters 6 and 7 in this book. Only a few NT setups exist in the world (see [4] for a review of facilities in Europe) because of the high neutron fluxes required to perform a full scan of an object in

a reasonable time. This has not prevented the successful application of NT to CH objects. Generally CH objects benefit from NT developments driven, example, by engineering applications. Figure 13.1 shows an example where the image contrast of an ancient Roman brooch is improved by using a cold neutron beam: the proportionality of neutron capture cross section to neutron wavelength is exploited to select the neutron wavelength that best matches the thickness and composition of the object. Imaging CH objects with neutrons offers unique opportunities: it permits the search for hydrogenous materials inside sealed metal objects, which is impossible with X-rays; it allows differentiation between elements close in the Mendeleev table, which would show the same contrast to X-rays; and finally, it enables differentiation between isotopes. The elemental information is inferred from the neutron attenuation. A typical example is a metal artifact, such as a statuette or a vase, in which different materials can be found in inserts or welds and provide useful information on the fabrication methods.

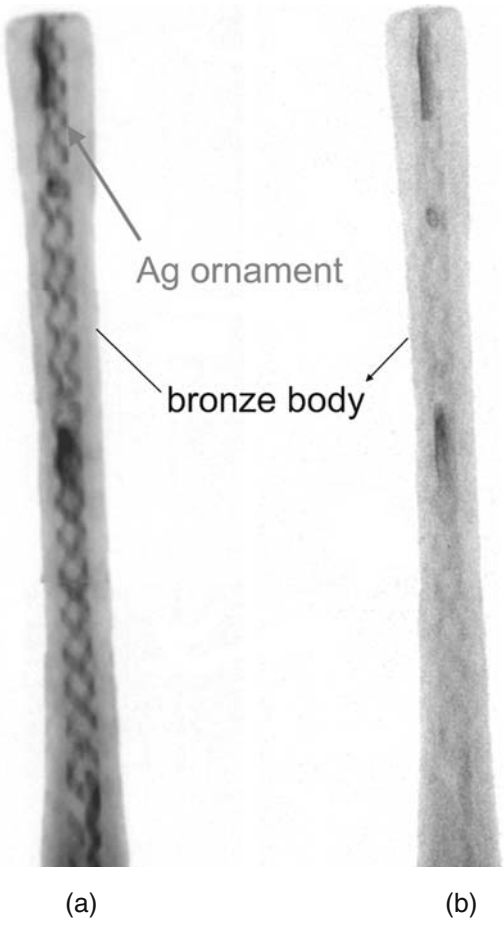

Fig. 13.1 Radiographs of an ancient Roman brooch taken with (**a**) cold neutron (5.5 Å) using a velocity selector at the Prompt Gamma-Ray Activation (PGA) station of the Paul Scherrer Institut (PSI), Switzerland [5] and (**b**) standard thermal (1.8 Å) neutron radiography technique at the Neutron Transmission Radiography (NEUTRA) station at PSI [6]

In the cold/thermal neutron energy range, the elemental sensitivity of neutron imaging can be enhanced using Bragg cutoffs (or Bragg edges). At a so-called Bragg cutoff wavelength, the neutron attenuation coefficient drops drastically. If the drop in attenuation is important and one can monochromatize the beam and select its wavelength, this behavior can be exploited to change the material contrast. Indeed, if two radiographs are taken, one with a wavelength just below the Bragg cutoff of a selected element and one with a wavelength just above it, the ratio will be sensitive to this element only. On the other hand, if two wavelengths are selected where the attenuation coefficient is equal, the element disappears in the ratio of the two radiographs as well as in the tomographic result (Fig. 13.2) [5]. This dichromatic tomography method has been demonstrated both at reactor sources and at pulsed neutron sources. It is similar to what can be done with X-rays using the rise in attenuation at the K-edge energy [7] (Fig. 13.3). Both methods can in principle provide a 3D map of a selected element. However, not all elements have Bragg edges, and only elements with high atomic number, which have the K-edge at high X-ray energy, can be imaged in large samples. Thus the use of Bragg edges and K-edges represents a step forward, but with limited scope.

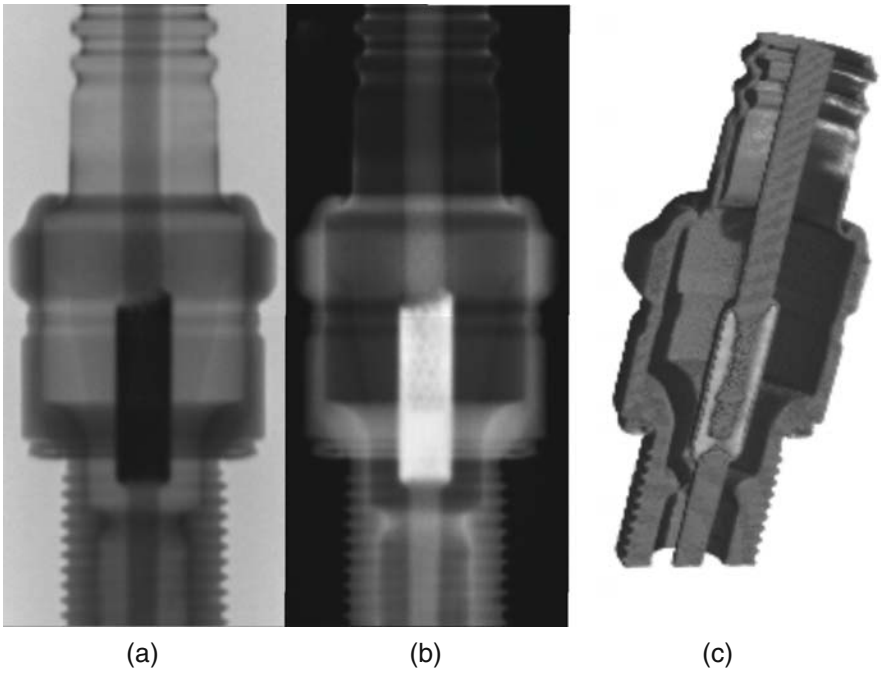

Fig. 13.2 (**a**) Neutron radiograph of a spark plug at 6.9 Å; (**b**) result of the division of two radiographs, one at 6.9 Å and the other at 3.2 Å, showing that the steel cladding (central part) became transparent; (**c**) 3D result of dichromatic tomography. Detailed explanations can be found in [5]

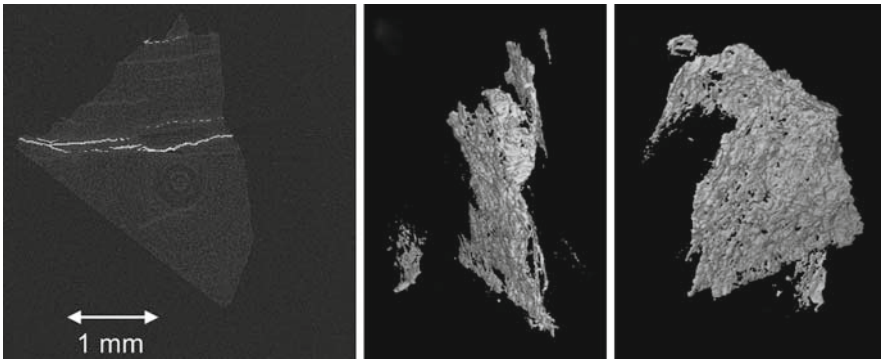

Fig. 13.3 A gold-sensitive tomography of an ore of Ashanti (Ghana) origin performed at the high-energy beam line (ID15) of the European Synchrotron Radiation Facility (Grenoble, France) shows that thin (about 40 μm) but extended layers (gold veins) appear in the quartz beads [7]: (**a**) shows a horizontal cut in the tomography made at 80 keV, where the gold veins and the quartz matrix are visible on top of ring-shaped reconstruction noise; (**b**) and (**c**) are two different 3D views of the result of the dichromatic tomography, sensitive to gold only.

Bragg edges may be more useful for CH applications because of the texture information embedded in their detailed shapes. Texture in the phases distorts the Bragg edges, so it can be used as a fingerprinting technique with the potential for texture mapping [8]. Appropriate transmission detectors need to be developed before this technique can be used routinely at pulsed neutron sources. On the other hand, phase-sensitive neutron diffraction (ND) techniques are in regular use for phase and microstructure characterization of ceramic and bronze artifacts, including texture analysis (see below). Texture provides important clues to the deformation history and thus to historic production steps, a prominent example being the neutron texture analysis of the early Copper Age Iceman axe [9].

Three features of neutron interactions with nuclei are exploited to provide analytical tools to determine the elemental compositions of CH objects:

1. radioactive nuclei produced by thermal/cold neutron capture,
2. prompt gamma rays from thermal/cold neutron capture, and
3. resonant neutron absorption at element-specific neutron energies in the epithermal energy range.

The first feature has long been exploited by a method known as neutron activation analysis (NAA). It started with the detection of radioactive isotopes through their half-lives. Now, these isotopes are observed and quantified with high-resolution gamma-ray detectors on the basis of gamma-ray energies as well as gamma-ray half-lives. This technique, known as instrumental neutron activation analysis (INAA), is now a valuable analytical tool for CH studies in use at many facilities [10, 11]. INAA may be invasive because it may require the

preparation of a small sample (e.g., powder) of the object before irradiation in a reactor. A related noninvasive imaging method is neutron activation autoradiography (NAAR) [12], in which two-dimensional (2D) objects are exposed to cold neutrons and the map of the neutron-induced gamma activation is recorded at different times by radiographic methods. NAAR is limited to 2D objects but is a unique tool for the investigation of paintings.

For the noninvasive elemental imaging of 3D objects, features (2) and (3) in the list above, which provide the basis for recently developed analytical methods, should be considered. Prompt gamma-ray activation analysis (PGAA) is based on the detection of characteristic gamma-ray energy spectra during thermal/cold neutron capture. It provides a nondestructive determination of the elemental (isotopic) composition of CH objects with good sensitivity to both major and trace elements. Mainly developed by G. Molnár and coworkers at the Budapest research reactor [13], PGAA has found many applications and has reached a high level of sophistication. Neutron resonance capture analysis (NRCA) was developed as a new analytical tool by H. Postma and coworkers at the GELINA pulsed neutron source [14]. NRCA makes use of the unique resonance absorption properties of epithermal neutrons. Many elements found in common CH materials have neutron absorption resonances in the energy range below 1 keV, including copper, cobalt, silver, tin, antimony, and gold. The gamma rays from resonant neutron capture are detected as a function of time, that is of neutron velocity. The time spectrum has emission peaks at element-specific resonance energies. Calibration of the gamma-ray detector array using reference samples is used to convert the resonant gamma-ray yield into absolute elemental composition. An alternative approach is also possible in which the neutron transmission through an object is measured instead of the gamma-ray emission. The transmitted neutron spectrum of a pulsed neutron beam has characteristic resonance dips in the time spectrum that can be used to determine the elemental composition of the object in the same way as the resonance peaks of NRCA.

PGAA and NRCA are well-established nondestructive methods for bulk analysis of CH objects, with sensitivities that can reach the parts-per-million range. There is no important reason why the spatial resolution of PGAA, NRCA, and neutron transmission methods should not be improved, eventually leading to nondestructive measurement with good spatial resolution of the composition (major and trace elements) of small parts inside a large object. These 3D extensions of PGAA and NRCA are presented in this chapter as a new development that can fill the gaps between 3D imaging, surface analyses, and bulk analyses. In the following discussion, the 3D extensions will be called prompt gamma-ray activation imaging (PGAI), neutron resonance capture imaging (NRCI), and neutron resonance transmission (NRT) tomography. PGAI, NRCI, and NRT are unlikely to achieve the spatial resolution obtained by conventional NT. It is the combined use of these new imaging techniques with neutron and X-ray tomographies that we foresee as the way forward in neutron imaging. Another development foreseen is 3D imaging of crystalline

phases (neutron diffraction imaging, NDI), which can essentially be undertaken using existing diffraction instruments. These methods together are expected to provide a new, comprehensive neutron-based approach that could be used for 3D imaging of the elemental and phase compositions of CH objects.

Interestingly, this is a rare case of a new development in neutron instrumentation that is motivated by CH applications. The new imaging techniques are being developed within the Ancient Charm (AC)[1] project, a collaboration of ten universities, central laboratories, and cultural heritage institutions across Europe [15]. A technical challenge of the project is represented by the need to perform high-efficiency gamma-ray measurements in a neutron environment, with the associated background, and to extend spatially resolved neutron transmission measurements into the epithermal range. The underlying techniques are presented in more detail in this chapter together with highlights of recent developments and CH applications.

13.2 Two Neutron Beam Analytical Techniques: Neutron Resonance Capture Analysis and Prompt Gamma-Ray Activation Analysis

13.2.1 Neutron Resonance Capture Analysis

Neutron resonance capture analysis makes use of the unique resonance absorption properties of epithermal neutrons for analyzing the bulk composition of materials and objects. The absorption cross sections of most elements are well known; they vary from one element to another and actually vary between isotopes of the same element [16]. Neutron absorption is followed by the prompt emission of a gamma-ray cascade with total cascade energies of up to about 8 MeV. The detailed energy spectrum of the gamma emission is also well known in the case of thermal neutron capture, but it can vary among resonances. NRCA is used at the GELINA pulsed neutron source for analysis of CH artifacts to determine the concentration of neutron-sensitive elements [17–25].

So far NRCA has been applied to a large number of artifacts, mainly bronze objects. A typical NRCA spectrum looks like the one in Fig. 13.4 [25] obtained by exposing an Etruscan votive object to the GELINA neutron beam. A number of resonance peaks of different elements (copper, lead) are clearly visible, corresponding to neutron energies in the range from 3,250 to 3,650 eV. The energies and intensities of the resonance peaks characterize the elemental composition of the sample. Figure 13.4 shows the 3,357 eV resonance of lead-206 and three copper resonances at 3,310, 3,503, and 3,588 eV. Because

[1] Ancient Charm (Analysis by Neutron Resonant Capture Imaging and other Emerging Neutron Techniques: Cultural Heritage and Archaeological Research Methods), http://ancient-charm.neutron-eu.net/ach.

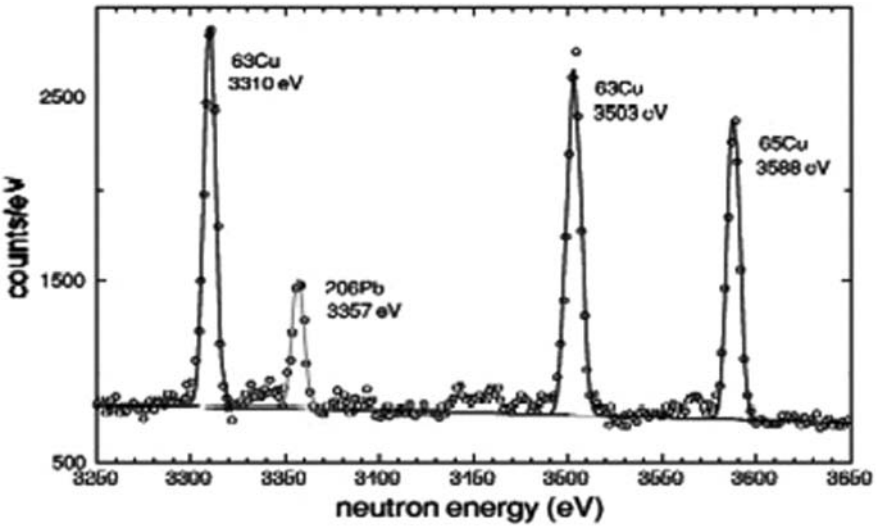

Fig. 13.4 Example of neutron resonance capture analysis NRCA spectrum featuring three copper resonances and one lead resonance in the region of 3,250–3,650 eV used to determine the Pb/Cu weight ratio of an Etruscan votive object [25]

these four resonances are weak, the Pb/Cu weight ratio can be obtained after small self-shielding corrections. A set of Etruscan statuettes from a collection originally owned by Earl Corazzi of Cortona (Tuscany), now at the National Museum of Antiquities in Leiden (Netherlands), are among the objects investigated by NRCA. In this case, NRCA was used to distinguish suspected fakes from genuine statuettes, solely on the basis of the elemental compositions of the artifacts [20]. The conclusion was based on the observation that minor quantities (up to several percent) of zinc occurred in some of these statuettes. Given the melting techniques available to the Etruscan blacksmiths, no more than a fraction of a percent of zinc would occur in a genuine artifact (Fig. 13.5).

13.2.2 Prompt Gamma-Ray Activation Analysis

Prompt gamma-ray activation analysis is a nondestructive nuclear method for performing both qualitative and quantitative multielement analysis of major, minor, and trace elements in samples. The technique is useful for the analysis of light elements such as H, B, C, N, Si, P, S, and Cl, as well as for heavy elements such as Cd, Sm, Gd, and Hg [26]. When a thermal or cold neutron is absorbed by a target nucleus, the compound nucleus is in an excited state with energy equal to the binding energy of the added neutron. Then the compound nucleus will almost instantaneously (in less than 10^{-14} s) de-excite into a more stable configuration through the emission of characteristic prompt gamma rays. In many cases, this new configuration yields a radioactive nucleus that also de-excites (or decays) by

Fig. 13.5 Photograph of two Etruscan statuettes, one genuine and one false [20]

emission of characteristic delayed gamma rays. PGAA is based on the detection and quantification of the prompt gamma rays emitted by the sample during neutron irradiation, while NAA uses the delayed gamma rays from the radioactive daughter nucleus (Fig. 13.6). Consequently, PGAA complements NAA by allowing determination of elements that do not form radioactive products after irradiation (e.g., hydrogen and boron) and elements for which the half-life is too long to be conveniently measured by NAA (e.g., carbon). Boron is the only exception to the

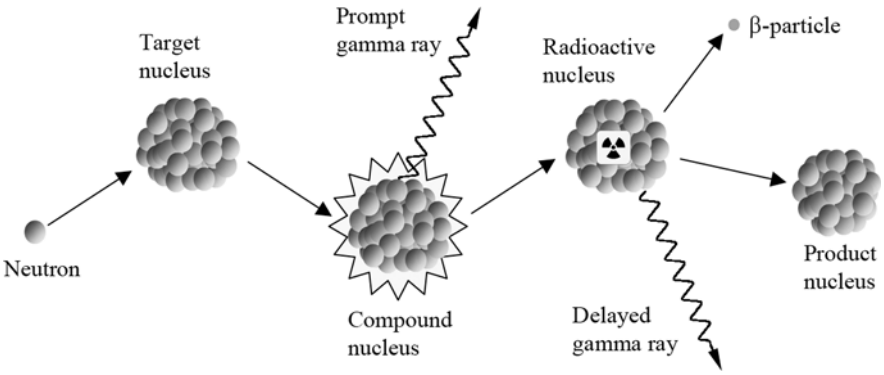

Fig. 13.6 Nuclear processes involved in prompt gamma-ray activation analysis (PGAA) and neutron activation analysis (NAA): neutron capture is immediately followed by emission of prompt gamma rays. The compound nucleus decays by beta emission followed by the emission of delayed gamma rays

usual prompt gamma-ray measurements in that the gamma measured is not due to the (n, γ) reaction. Indeed, boron (like lithium-6) reacts with neutrons by emission of α-particles [i.e., via the reaction ^{10}B(n, α)^{7}Li]. Most of the lithium-7 is formed in an excited state and de-excited instantaneously (within 10^{-14} s) by the emission of 477 keV gamma rays.

The PGAA technique requires mainly a source of thermal or cold neutrons and a high-resolution spectrometer for measurement of gamma rays with energies over a range from about 100 keV to 11 MeV. The energies of the prompt gamma rays identify the neutron-capturing elements, while the intensities of the peaks at these energies are used to determine their concentrations (Fig. 13.7). An advantage of the PGAA method is that nothing special is required in the way of sample preparation: the sample can be in a solid, liquid, or gaseous state. Depending on the amount of the investigated material,

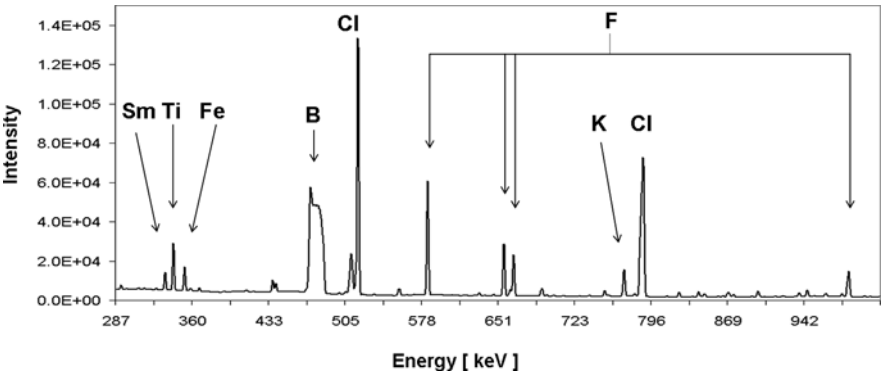

Fig. 13.7 Example of prompt gamma-ray activation analysis (PGAA) spectrum from an estuarine sediment

element, and target matrix, the detection limit for a PGAA installation can be as low as 10 ppb (for B, Sm, Gd). The activity of the object after irradiation is low or decreases rapidly in most cases; therefore, the object can be returned within a few days of the measurement. Compared with NAA, where the sample is placed close to the core of the reactor, the neutron beam intensity at the sample is six orders of magnitude lower.

A typical setup for PGAA consists of a sample box, a shielding, and a detection system [13, 27–30]. The object is exposed to an intense thermal or, preferably, cold neutron beam on the order of 10^6–10^8 n/cm^{2}s, originating from a neutron guide. The neutron guide is preferably curved to avoid a direct view to the moderator or cold neutron source, thus reducing the fast-neutron and gamma-ray background. The huge number of peaks in a spectrum (up to about a thousand) requires a high-purity germanium (HPGe) detector with high-energy resolution (<2 keV at 1,332 keV). Moreover, many high-energy gamma rays will not deposit their full energy inside the HPGe detector and thus build up large Compton tails that will hide peaks at lower energies or generate (unwanted) additional escape peaks. To reduce these effects, the HPGe detector is surrounded by a fast gamma-ray detector, usually made of an annular bismuth germanate oxide (BGO) or NaI(Tl) scintillator that serves to reject events simultaneously detected in the HPGe detector and the scintillator. This anti-Compton shield acts as an active shield against unwanted, external high-energy gamma rays that deposit part of their energy in the scintillator before scattering in the HPGe detector. The whole detection system is then covered with lead bricks and additional neutron shielding to further improve the signal/background ratio. The sample box is usually covered for the same reasons with lithium-6, except at the entry of the neutron beam, to prevent scattered neutrons from reaching the detector. The detection system is normally placed at 90° to the neutron beam.

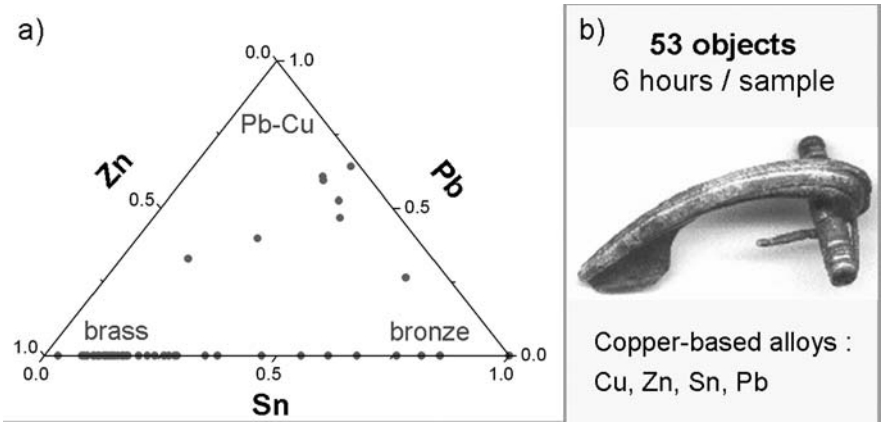

Fig. 13.8 Main composition of 53 brooches studied by S. Baechler et al. [31] (left) and a photograph of one of them (right)

The count rate of the acquisition system is limited to about 10 kHz by adjusting the neutron beam size with lithium-6 collimators.

PGAAs have been performed on various samples, in a wide range of fields, including material science, medicine, nuclear science, geology, and archeology. In one of the first CH applications, S. Baechler and coworkers [31] studied 53 La Tene and Roman brooches from western Switzerland and identified four different groups of copper-based alloys (Fig. 13.8).

13.3 Combined Prompt Gamma-Ray Activation Analysis Scanning and Neutron Tomography

The scope for upgrading a PGAA station to PGAI can be assessed by an estimate of the experimental time needed for a full scan of an object. The time needed to measure a $5 \times 5 \times 5\,cm^3$ object with a 1-mm^3 spatial resolution would be equal to 125,000 times the acquisition time to measure a 1-mm^3 sample. Limiting the acquisition time to 4 s—which is already a huge compromise because it takes from minutes to a few hours to analyze most samples using PGAA (to detect trace elements)—and estimating the time to move the object at 1 s, the total beam time would be more than a week. Unfortunately, objects with cultural importance are typically manufactured objects, made of numerous small parts, each of them being to some extent homogeneous. A complete scan at high spatial resolution of such objects would be not only impossible but also of little use. A better approach to the problem is to use another technique to distinguish the different parts of the object and then to measure them by PGAI, with an adequate spatial resolution smaller than an ideal level of detail but large enough to measure the main and minor elements in a reasonable length of time. The full process can be optimized further in the following way:

1. the object is imaged by X-ray tomography with a high spatial resolution, typically 10 μm;
2. an NT of the object is performed with a resolution down to 100 μm;
3. a bulk PGAA of the whole object is performed to identify all the elements present; and
4. the regions of interest are measured by PGAI.

The acquisition time is regulated by the requirements for quantifying the elements seen in the bulk analysis. Another limitation may come from the need to keep the induced long-lived activation of the object to an acceptable level; for CH objects this means returning the object to a curator after a few weeks. This is not a problem for PGAA but should be reconsidered in the case of trace elements exposed to large neutron fluences in PGAI.

Alternative geometrical arrangements can be considered in the implementation of PGAI. The first and preferred one consists in collimating the neutron beam using a 1-mm-thick lithium-6 foil with a hole that lets a neutron beam of the order

of 1 mm^2 to pass. A thick gamma-ray collimator made of lead, placed in front of the spectrometer, defines a pencil beam of gamma rays allowed to enter the spectrometer. The intersection of the neutron beam and the gamma-ray beam delimits a voxel, a region of the object measured by PGAI. With this solution, a 3D map of the composition of the object is obtained by scanning the object across the neutron beam and in front of the HPGe detector in three dimensions (XYZ). For each voxel, a gamma-ray spectrum is acquired and its analysis yields the composition of the small portion of the object, defined by the intersection of neutron beam collimation and HPGe collimation. An advantage of this solution is that one can in a simple way select the voxel and its size. Provided an X-ray and/or a neutron tomography of the object is performed before the PGAI measurements, the experiment can be as simple as the following: the user selects with the 3D visualization software the 3D coordinates of a region of interest (ROI) and a motorized 3D positioning stage places this ROI in front of the collimators for a PGAI measurement. In principle, the best orientation of the sample in the set of collimators can be found by minimizing the attenuation of neutrons in the path to the ROI and of the gamma rays in the path from the ROI to the detector.

This scanning solution presents the following drawbacks.

1. Neutrons scatter inside the object, especially if the object contains hydrogen, so the irradiated region is no longer a beam of 1 mm^2.
2. Collimation of high-energy gamma rays (>1 MeV) requires at least 20-cm-thick lead brick. This increases the distance between the object and the detection system, reducing its efficiency and thereafter increasing the acquisition time. A compromise again must be chosen between best collimation and measuring time. Fortunately, most emitted gamma rays have energies below 1 MeV.
3. Reducing the viewing cone of the spectrometer reduces not only the size of the ROI but also the efficiency of the detector. It does not, however, reduce the background.

An alternative solution that would improve the signal/background ratio of PGAI consists of removing the gamma-ray collimation. The object would be scanned in two dimensions with the neutron beam and rotated from 0 to 180°. This solution corresponds to prompt gamma-ray activation tomography in which the HPGe acquires spectra coming from lines though the object. Measuring the set of lines at different orientations of the object yields a 3D map of the composition of the object. The number of positions is larger than with the scanning solution. Indeed, keeping in mind our $5 \times 5 \times 5$ cm^3 object and a final spatial resolution of 1 mm^3, the required number of projections is slightly larger than for the scanning solution: $50 \times 50 \times \pi/2 \times 50 = 196{,}350$. The acquisition time is, on the other hand, more than 100,000 times shorter in a first approximation because the spectrometer views a $50 \times 1 \times 1$ mm^3 portion of the object, and the collimation in front of the detector can be released. The total measurement time would then be less than 3 days, dominated by the time to move the object.

The real disadvantage of this method is that it is not possible to determine the composition of a part of the object without measuring at least a full slice of it, as

required by the reconstruction algorithm. The a priori knowledge of the object structure from neutron or X-ray tomography is not in this case directly useable — the whole object must be measured regardless. A third option for implementation of PGAI would consist of keeping the gamma-ray collimation and not the neutron collimation. This solution reproduces single photon emission computed tomography, with spectra as projections; the reconstruction of the composition maps consists of reconstructing each element separately. This solution, however, does not make use of the main advantage of using cold neutrons (i.e., that one can easily collimate them and irradiate only a selected part of the object without reducing the total measurement time).

S. Baechler and coworkers performed the first PGAI experiment at the PGA station of Paul Scherrer Institut (PSI), Switzerland, to study a piece of the 2-billion-year-old Oklo natural reactor [32]. The cold neutron beam was focused using a neutron lens and reduced to 1 mm^2 by a lithium-6 collimator at the focal point. No collimator was placed in front of the HPGe detector, and the sample was scanned only in two dimensions in front of the neutron beam without rotations. Although they gave the composition integrated over the neutron path only, the results agreed with the uranium-sensitive tomography (Fig. 13.9) taken at the European Synchrotron Radiation Facility (Grenoble, France) using high-energy X-rays [7]. Besides the combinative use of two techniques to interpret PGAI results, this experiment showed that one could correct PGAI data for gamma-ray attenuation using the tomography results.

It is obvious from the simple calculation on the required measuring time that an intense cold neutron beam should be available to study large objects. A new PGAA facility [33] is now available at FRM-II[2] in Germany [34]. One of its major features is a super-mirror elliptic tapered neutron guide that should focus cold

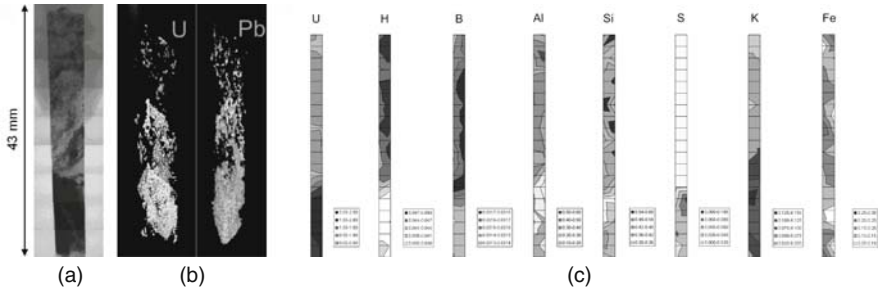

Fig. 13.9 (**a**) X-ray radiograph at 87 keV of a piece from the Oklo natural reactor (Gabon); (**b**) 3D distributions of lead and uranium resulting from tomographies taken at the high-energy beam line (ID15) of the European Synchrotron Radiation Facility (Grenoble, France) [7]; (**c**) spatial distributions of selected elements in the same piece, obtained by prompt gamma-ray activation imaging at the Paul Scherrer Institut (Villigen, Switzerland) [32]

[2] Forschungsreaktor München II (translation: Munich Research Reactor II), Munich Technical University.

neutrons to a spot size of $4 \times 7\,mm^2$ at 10 cm from the end of the guide. The cold neutron flux is expected to exceed 10^{10} n/cm^{2}s at the focal point [35]. One of the aims of the facility is to test different PGAI geometry options on CH objects.

13.4 Imaging with Neutron Resonances

The NRCA experience at the GELINA neutron source [17–25] is the starting point for the development of an imaging method based on resonant neutron capture. Imaging applications require high neutron fluxes, and the 100 times more powerful ISIS pulsed neutron source (Chilton, UK) is now used for the development of NRCI and NRT [15]. Figure 13.10 shows a sketch of the NRCI/NRT setup that is under construction at ISIS. In the case of NRCI, the object is scanned in front of a collimated neutron beam while a set of scintillator detectors surrounding the object record the capture gamma rays. The composition of the object must be retrieved by a tomographic reconstruction corrected for neutron self-absorption. In practice the spatial resolution is limited by the need to collimate the beam of epithermal neutrons while keeping the signal/background at an acceptable level. The best compromise at the moment seems

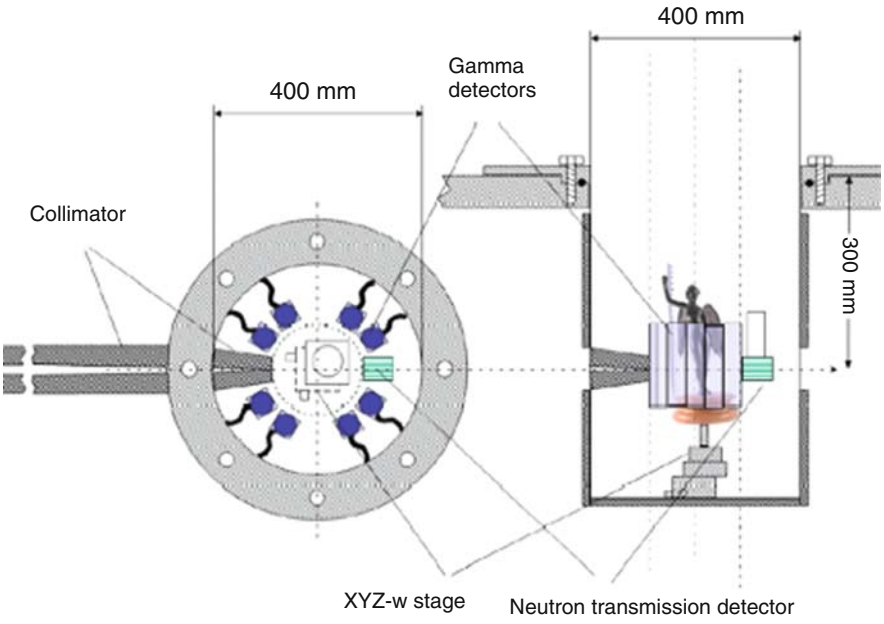

Fig 13.10 Sketch of a setup for performing neutron resonance capture imaging and neutron resonance tomography. The sample is attached to a frame allowing translation and rotation motion relative to the beam and detectors, which are fixed. The gamma-ray detectors for NRCI are placed around the sample. A position-sensitive detector for NRT is placed in the neutron beam behind the sample

to be a collimated beam diameter of 5 mm, which is also the anticipated spatial resolution to be achieved by NRCI in the ISIS experiment.

For NRT measurements, the neutron collimator is removed and the object is scanned and rotated in front of the NRT detector. Indeed the main challenge in NRT is the realization of a position-sensitive detector for epithermal neutrons suitable for time-of-flight (TOF) measurements. It is obvious that the spatial resolution of such a detector will not reach, in the near future, the resolution of the ones used in thermal or cold NT. The detector prototype tested at ISIS [36] features 2×2 mm^2 pixels made from lithium glass. A length of 8 mm for each pixel provides adequate efficiency for epithermal neutron detection, and an array of 10×10 pixels can be managed. Thus NRT is expected to provide better spatial resolution than NRCI in a much shorter time. It may, however, have lower sensitivity to trace elements, as suggested by the GELINA experience, where transmission measurements are in regular use for total neutron cross section measurements. Compared with NT, NRCI and NRT have a coarse spatial resolution but provide direct information on the elemental composition; NT provides composition information only indirectly via energy analysis of neutrons. An interesting observation is that the information acquired by the NRT detector is much richer than a radiograph: a full TOF spectrum per pixel with several resonances per element is measured, yielding several element-sensitive images at once. The NRT potential is better understood in the case of large samples. With thermal or cold NT, when the sample is "black" (i.e., too thick or too absorbing), there is no way to image it. With NRT, there are often many resonances for one or more elements in the object. An object may be black for one resonance but could still be imaged with another resonance in the spectrum. The NRT detector can also be used in the thermal energy range to provide, for example, strain and texture information using Bragg edge analysis to complement neutron diffraction imaging (NDI) studies. The ISIS experience will tell us to what extent the potential of the new NRCI/NRT device under construction can be exploited to provide 3D maps of the elemental and phase composition of CH objects.

From the descriptions of the different techniques PGAA, NRCA, PGAI, NRCI, NT, and NRT, one may conclude that an appropriate combination of all of them, along with NDI, can be the basis for integrated analysis protocols for the study of CH objects. The integrated use of imaging and other neutron-based techniques for CH studies is indeed an area of ongoing research, as illustrated by the applications discussed below.

13.5 Applications to Cultural Heritage Studies

In the past few years, neutron techniques have increasingly been used for the study of CH materials, in particular to address their nature and authenticity, their provenance and diffusion, the manufacturing techniques used in their fabrication, and their state and conservation [37]. In the following discussion, we show first results from the AC project [38–41] and examples of applications

of thermal and cold neutron tomographic techniques to the study of phase and microstructure characterization of ceramic artifacts, ancient bronzes, and marble artifacts. A common feature in the selected examples is that the use of neutrons was motivated either by the general aim of developing new imaging techniques or by the need to perform a nondestructive analysis. Cast and restored metal objects were inspected to elucidate the production technology and the corrosion damage. Marble and ceramic artifacts were inspected to probe the presence of adhesives, glued parts, epoxy filler materials, or epoxy protective coatings.

For testing purposes, the AC archaeologists prepared "black boxes." These closed metal cubes contain objects of various shapes, forms, and elemental composition representative of the composition of real archaeological objects. The task was to recognize the elemental composition and the rest–strain of the inner objects by PGAI, NRCI, and NDI [38–41]. Neutron and X-ray radiography and tomography were used to visualize the inner content of the black boxes and to help with targeting the coordinates of the interesting spots for the new 3D neutron techniques. NT was performed at the ANTARES[3] facility [42] at FRM-II, and the X-ray tomographies were performed at the Centre for X-ray Tomography at the Ghent University [43]. Figure 13.11 shows a 3D visualization (tomograph) of the reconstructed X-ray data (a) and the corresponding neutron data (b) for one of the black boxes. Using solely the image content, it can be seen that neither X-ray tomography nor NT alone allows the derivation of both types of materials and the elemental composition of the scanned object. However, the

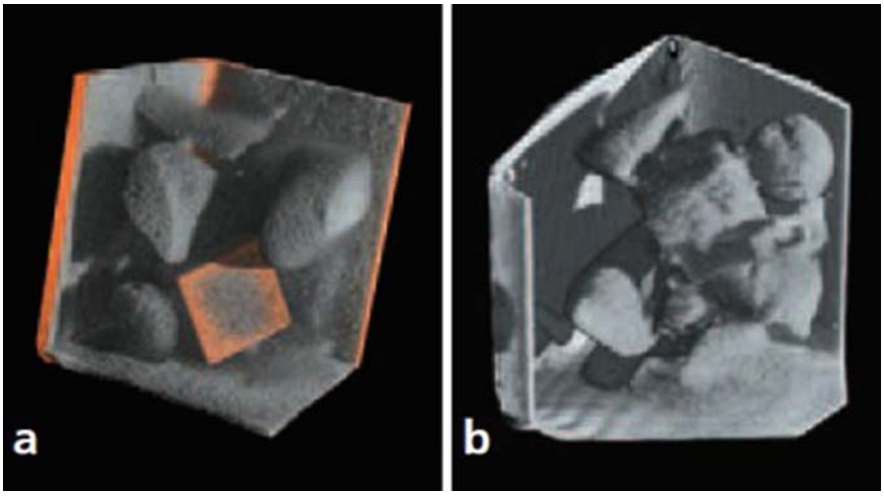

Fig. 13.11 X-ray tomograph (**a**) and neutron tomograph (**b**) of black box H-IX from the Ancient Charm project [39]

[3] Advanced Neutron Tomography and Radiography Experimental System.

combined use of the two techniques allows areas of differing materials and their shapes to be distinguished and separated. At a later stage, to determine precisely the elemental composition of these objects, PGAI analysis was performed directly at the coordinates provided by the NT image. Figure 13.12 shows an X-ray tomograph and the corresponding neutron tomographs for another black box. Here three separate layers of materials can be visually distinguished. The upper row shows corresponding horizontal slices of the object (looking "from above"); the bottom row shows vertical slices (looking "from the side"). A suitable isocontour of the X-ray slice helps in visualizing the initial misalignment of the NT image and its correct alignment after the registration. This example demonstrates in various ways the value added by the registration and the subsequent point-to-point comparison.

The neutron tomograph in Fig. 13.13 refers to laminated bronze artifacts from rich sepulchral complexes in the necropolis of *Osteria-Poggio Mengarelli* and *Cavalupo* (eighth century B.C.) [44]. Quantitative phase analysis was performed by neutron diffraction at the INES[4] diffractometer installed at the ISIS neutron source. This result was complemented by the analysis of the spatial distribution of the components, obtained with an NT experiment (Fig. 13.13),

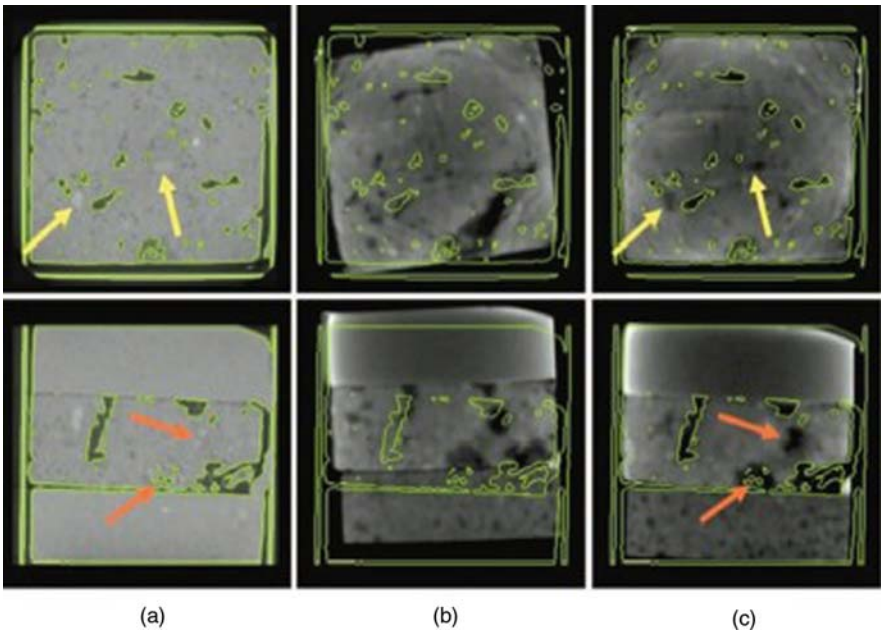

Fig. 13.12 (a) X-ray tomograph of black box D-VIII from the Ancient Charm project [39]; corresponding neutron tomograph in the initial position (**b**) and after automatic registration (**c**) [38]

[4] Italian Neutron Experimental Station, a collaborative project between ISIS and the Italian National Research Council [Consiglio Nazionale delle Ricerche].

Fig. 13.13 Neutron tomography from bronzes [44] provided information on the spatial distribution of the components forming the samples. Measurements were performed at the COld Neutron RADiography (CONRAD) instrument at the Hahn-Meitner Institut (Berlin, Germany)

and additional information on elemental composition through XRF. A surface photomicrograph and infrared scan were used to complete the characterization of the bronzes.

The results in Fig. 13.14 refer to marbles from Villa Adriana [45, 46] for which the geological setting is a priori unknown. Marble is typically composed of carbonate minerals (such as calcite and dolomite), silicates (such as quartz, plagioclase and micas), oxides (such as rutile and magnetite), and phosphates (such as apatite) can be present as trace or minor phases. Natural calcite rocks and marbles commonly exhibit a preferred orientation (texture), which forms during growth or deformation and which is modified during recrystallization and plastic tectonic deformations. These geological textures, formed over millions of years, are not affected by quarrying or stone sculpting. Thus, in the archaeological context, the texture analysis of marble helps in attribution and provenance determination. It may further be useful in the field of conservation: for instance, the weathering of marble by anisotropic thermal expansion is also influenced by the crystallographic textures [47]. Based on references [45, 46], it was possible to distinguish among the different marble types purely on the basis of the mineral phase compositions and the crystallographic textures (geological stress). In particular, the phase analysis performed on the Villa Adriana marble fragments allows for a clear separation into four different groups. The same marbles were also investigated by thermal NT (Fig. 13.15). From this study, it was possible to distinguish distinct components and their relative spatial distributions in the marbles. These are indicated with different colors in the tomographic picture in Fig. 13.15. (a) darkest shade (most abundant component), (b) medium shade (intermediate component), and (c) lightest shade (smaller component) (courtesy of R. Triolo et al. [48]).

Finally, ceramic artifacts dated from the second to the third century (A.D.) from a large collection found in recent excavations (1988) in Puglia (Italy) were investigated. Their provenance is different areas of the central Mediterranean. Neutron diffraction and NT measurements [48] performed respectively at the ISIS pulsed neutron source and at PSI [49] provided valuable information on composition, provenance, and fabrication methods. Samples were found to be made of the same type of clay, with similar percentages of calcite, quartz, and

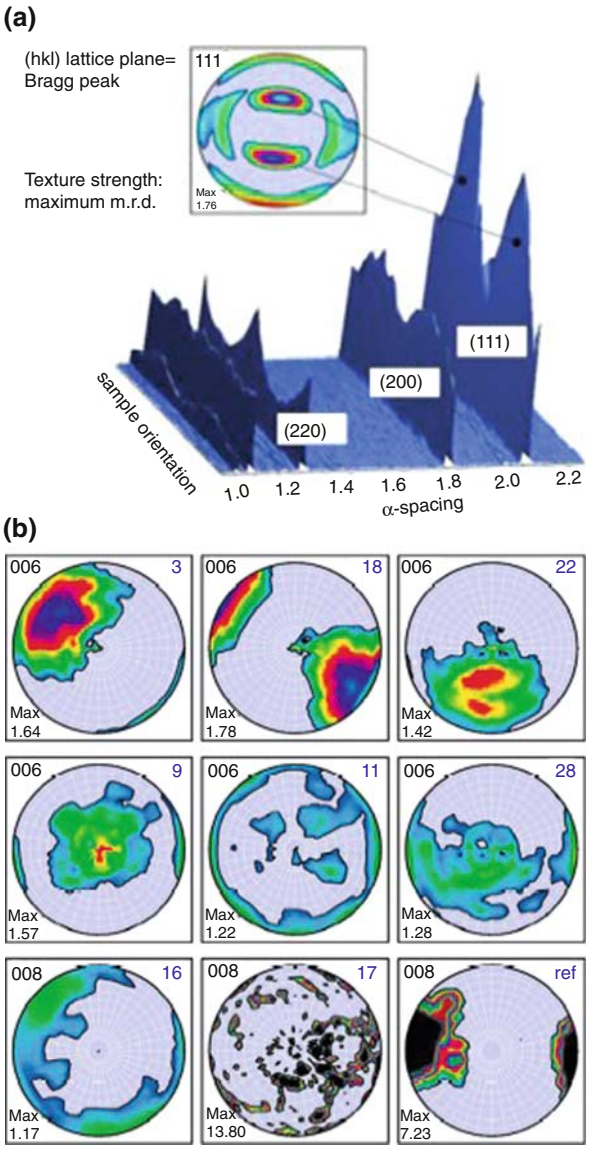

Fig. 13.14 (**a**) Example of texture analysis of a copper reference sample derived from diffraction data on the ROTAX instrument installed at ISIS (courtesy W. Kockelmann); (**b**) Maps of the c-axis distributions, represented by the (006) pole figures, of eight distinct marble samples from Villa Adriana [45] compared with a geological calcite reference sample from Syros, Greece. For each pole figure, the maximum multiples of random distribution are given

plagioclase. The examples in Fig. 13.16 demonstrate that a 3D inside view of objects a few centimeters thick can be achieved within a relatively short time (from a few minutes to a few hours) with spatial resolution of as low as 100 μm. The characterization of a ceramic artifact and the analysis of the composition of alloys in a metallic object provided an additional piece of information to aid in establishing whether the object belonged to the history of the local people or was imported from another culture [50].

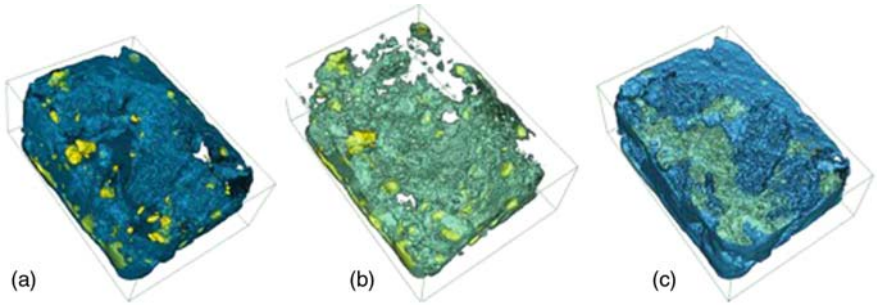

Fig. 13.15 Example of neutron tomography of marble fragments from Villa Adriana [48]

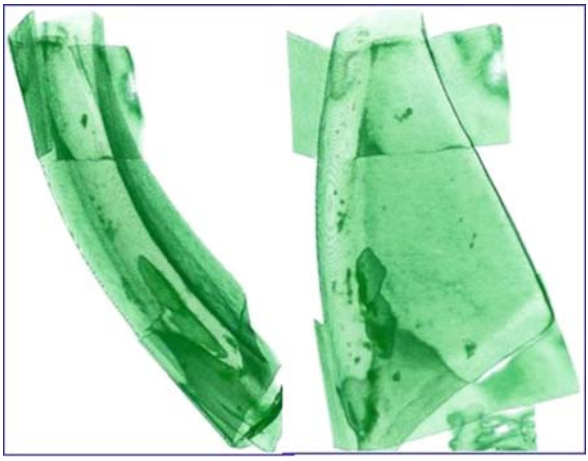

Fig. 13.16 Example of neutron tomography from ceramic artifacts [48]

The characterization by neutron diffraction of ancient bronze, marble, and ceramic artifacts illustrates how the penetrating power of neutrons, combined with imaging analysis, leads to advances in the scientific characterization of the materials that constitute a CH object. The techniques used are truly nondestructive, an important advantage if a unique and precious artifact is to be investigated without risk of damaging it in the analysis. The ongoing developments in applications of neutrons in CH research are promising and suggest that neutron-based techniques will have a lasting impact on the way CH analyses are performed. This will be especially the case if comprehensive analysis protocols are developed and adopted as best practices by the CH community.

Acknowledgment This work was performed with financial support from the European Community under contract HPRI-2001-50043 and within the CNR-Council for the Central Laboratory of the Research Councils (UK) agreement. Carla Andreani and Giuseppe Gorini acknowledge Consiglio Nazionale delle Ricerche (CNR), Italy, for financial support for the experiments performed at ISIS. Thomas Materna acknowledges financial support from the

Swiss National fund, the University of Fribourg (Switzerland), and the University of Cologne (Germany) for the experiments performed at PSI and the European Synchrotron Radiation Facility. We also wish to thank Giulia Festa for critical revision of the text.

References

1. Portal (News and developments from the CCLRC). *Looking forward to the past: science and heritage*. Special issue Autumn/winter (2006). http://www.scitech.ac.uk/Publications/nl/Portal/.
2. ESRF Newsletter. *Science and art*. **44** (December 2006).
3. M. Menu et al., The dedicated accelerator-based IBA facility AGLAE at the Louvre, *Nucl. Instrum. Meth. Phys. Res. B* **45**, 610–614 (1990).
4. E.H. Lehmann, P. Vontobel, B. Schillinger, T. Bücherl, S. Baechler, J. Jolie, W. Treimer, R. Rosa, G. Bayon, S. Legoupil, S. Körner, V. Micherov, M. Balasko, in *Proceeding of the 15th World Conf. on Non-Destructive Testing*, Rome, Italy, October 15–21, (2000). Available from http://www.ndt.net/article/wcndt00/papers/idn804/idn804.htm.
5. N. Kardjilov, S. Baechler, M. Bastürk, M. Dierick, J. Jolie, E. Lehmann, T. Materna, B. Schillinger, P. Vontobel, *Nucl. Instrum. Meth. Phys. Res.* A **501**, 536 (2003).
6. NEUTRA: Thermal neutron facility for imaging at the Paul Scherrer Institute, Villigen, Switzerland http://neutra.web.psi.ch/facility/index.html.
7. T. Materna et al., Uranium-sensitive tomography with synchrotron radiation, *J. Synchrotron Rad.* **6**, 1059–1064 (1999).
8. W. Kockelmann, G. Frei, E.H. Lehmann, P. Vontobel and J.R. Santisteban, *Nucl. Instrum. Meth. Phys. Res. A* **578**, 42 (2007).
9. G. Artioli, M. Dugnani, I. Angelini, L. Lutterotti, A. Pedrotti, A. Fleckinger, *Proc. Archaeometallurgy Europe* **2**, 19–27, (2003); G. Artioli, M. Dugnani, T. Hansen, L. Lutterotti, A. Pedrotti, G. Sperl, in: A. Fleckinger (ed.), *La mummia dell'età del rame. 2. Nuove ricerche sull'uomo venuto dal ghiaccio*, Vol. 3, Folio Verlag, Bolzano, 9–22, (2003).
10. E. Ciliberto and G. Spoto (eds.) *Modern Analytical Methods in Art and Archaeometry*, John Wiley & Sons, Inc. New York (2000).
11. D.R. Brothwell and A.M. Pollard (eds.) *Handbook of Archaeological Sciences*, John Wiley & Sons, Inc., New York (2001).
12. C.O.Fischer et al, Neues zur Neutronen-Aktivierungs-Autoradiographie, *Restauro* **105**, 426 (1999) (in German).
13. Zs. Révay and T. Belgya, Principles of the PGAA method, in G.L. Molnár ed., *Handbook of Prompt Gamma Activation Analysis with Neutron Beams*, Kluwer Academic Publishers, pp. 1–305 (2004).
14. H. Postma, M. Blaauw, P. Bode, P. Mutti, F. Corvi and P. Siegler, Neutron-resonance capture analysis of materials, *J. Radioanal. Nucl. Chem.* **248**(1), 115–120 (2001).
15. G. Gorini for the Ancient Charm collaboration, Ancient Charm: A research project for neutron-based investigation of cultural-heritage objects, *Il Nuovo. Cimento. C*, **30**, 47–58 (2007).
16. S.F. Mughabghab et al., *Neutron Cross-sections*, vol.1, Academic Press, New York (1981). Available online at http://atom.kaeri.re.kr/cgi-bin/endfplot.pl.
17. H. Postma, M. Blaauw, P. Schillebeeckx, G. Lobo, R. Halbertsma and A.J. Nijboer, Non-destructive elemental analysis of copper-alloy artefacts with epithermal neutron-resonance capture, *Czech. J. Phys.* **63**(Suppl. A), A233–A240 (2003).
18. M. Blaauw, H. Postma, P. Mutti, An attempt to date an antique Benin bronze using neutron resonance capture analysis, *Appl. Radiat. Isot.*, **62,** 429–433 (2005).
19. M. Blaauw, H. Postma and P. Mutti, Quantitative neutron capture resonance analysis verified with instrumental neutron activation analysis, *Nucl. Instrum. Meth. Phys. Res. A* **505**, 508–511 (2003).

20. H. Postma, P. Schillebeeckx, and R.B. Halbertsma, Neutron resonance capture analysis of some genuine and fake etruscan copper-alloy statuettes, *Archaeometry* **46** 635–646 (2004).
21. H. Postma and P. Schillebeeckx, Non-destructive analysis of objects using neutron resonance capture, memorial issue Gabor Molnár, *J Radioanal. Nucl. Chem.* **265,** 297–302 (2005).
22. R. C. Perego, H. Postma, M. Blaauw, P. Schillebeeckx, A. Borella, Neutron Resonance Capture Analysis: improvements of the Technique for resonances above 3 keV and new applications, *J. Radioanal. Nucl. Chem.* **271**(1) 89–94 (2007).
23. H. Postma, R.C. Perego, P. Schillebeeckx, P. Siegler, and A. Borella, Neutron resonance capture analysis and applications, *J. Radioanal. Nucl. Chem.* **271**(1) 95–99 (2007).
24. H. Postma, D. Fontijn, P. Schillebeeckx, R.C. Perego, and J.J. Butler, Neutron Resonance Capture Analysis of Geistingen axes, LUNULA, *Archaeologia protohistorica* **XIII**, 41–46, (2005).
25. H. Postma and P. Schillebeeckx, Neutron-resonance capture as a tool to analyse the internal compositions of objects non-destructively, *Notiziario Neutroni e Luce di Sincrotrone* **11**(2), 14–18 (2006).
26. Z.B. Alfassi, C. Chung (Ed.), *Prompt Gamma Neutron Activation Analysis*, CRC Press, Boca Raton, Florida, 1995.
27. M. Crittin et al. The new prompt gamma-ray activation facility at the Paul Scherrer Institute, Switzerland, *Nucl. Instr. Meth. Phys. Res. A* **449**, 221 (2000).
28. Zs. Revay et al., Cold neutron PGAA facility at Budapest, *Nucl. Instrum. Meth. Phys. Res. B* **213**, 385–388 (2004).
29. H-J Cho et al., Study on prompt gamma-ray spectrometer using Compton suppression system, *Nucl. Instrum. Meth. Phys. Res. B* **229**, 499–507 (2005).
30. Zs. Revay et al., Construction and characterization of the redesigned PGAA facility at the University of Texas at Austin, *Nucl. Instrum. Meth. Phys. Res. A* **577**, 611–618 (2007).
31. S. Baechler et al. The k0-method in cold-neutron prompt gamma-ray activation analysis, *J. Radioanal. Nucl. Chem.* **256**, 239–245 (2003).
32. S. Baechler et al., Non-destructive analysis of a bulky sample from a natural fossil reactor, *J. Radioanal. Nucl. Chem.* **250**, 39–45 (2001).
33. P. Kudejova et al., On the construction of a new instrument for cold-neutron prompt gamma-ray activation analysis at the FRM II, *J. Radioanal. Nucl. Chem.* **265**, 221–227 (2005).
34. Research reactor II (FRM-II), Technische Universität München, 2007 http://www.frm2.tum.de/en/index.html.
35. P. Kudejova, *Two new installation for non-destructive sample analysis: PIXE and PGAA*, Ph.D. Thesis, University of Cologne (2005).
36. E. Perelli Cippo et al, *Meas. Sci. Technol.* **19**, 034027 (2008).
37. W. Kockelmann, L.C. Chapon, R. Engels, j. Schelten, C. Neelmejer, H.M. Walcha, G. Artioli, S. Schalev, E. Perelli Cippo, M. Tardocchi, G. Gorini, and P. Radaelli, Neutrons in cultural heritage research, *J. Neutron Res.* **14**(1), 37–42 (2006).
38. P. Kudejova, J. Cizek, R. Schulze, J. Jolie, B. Schillinger, K. Lorenz, M. Mühlbauer, B. Masschaele, M. Dierick, J. Vlassenbroeck, A marker-free 3D image registration for the Ancient Charm project. Case study with neutron and X-ray tomography datasets, *Notiziario Neutroni e Luce di Sincrotrone* **12**(2), 6–13 (2007).
39. P. Kudejova for the Ancient Charm collaboration, Neutron and X-ray imaging of the 'black boxes' for the Ancient Charm project, *Archeometriai Műhely*, 35–40 (2008/1).
40. G. Festa, W. Kockelmann, A. Kirfel and the Ancient Charm collaboration, Neutron diffraction analysis of 'black boxes', *Archeometriai Műhely* 2008/1 61–72.
41. Z. Kis et al., Prompt gamma activation imaging on 'black boxes' in the 'Ancient Charm' project, *Archeometriai Műhely*. 41–60 (2008/1).
42. ANTARES *Facility at the research reactor II (FRM-II)*, Technische Universität München (2007). http://www.physik.tu-muenchen.de/antares/.

43. *X-ray Radiography and Tomography Facility at the Ghent University (UGCT)* (2007) http://www.ugct.ugent.be.
44. G. Festa, P.A. Caroppi, A. Filabozzi, C. Andreani, M.L. Arancio, R. Triolo, F. Lo Celso, V. Benfante, S. Imberti, Composition and corrosion phases of Etruscan Bronzes from Villanovan Age, *Measur. Sci. Technol.* **19**(3) 034004 (7 pp) (2008).
45. A. Filabozzi, A. Pietropaolo, C. Andreani, M. P. De Pascale, G. Gorini,.W. Kockelmann, L.C. Chapon, Non invasive neutron diffraction analyses of marbles from the "Edificio con Tre Esedre" in Villa Adriana, *Il Nuovo Cimento C* **29**, 237–252 (2006).
46. A. Filabozzi, C. Andreani, M.P. De Pascale, G. Gorini, A. Pietropaolo, E. Perelli Cippo, R. Senesi, M. Tardocchi and W. Kockelmann, Texture and structure studies on marbles from Villa Adriana via neutron diffraction technique, *J. Neutron Res.* **14**, 55–58 (2006).
47. S. Siegesmund and K. Ullemeyer, T. Weiss, and E.K. Tschegg, *Int. J. Earth Sci.* **89**, 170 (2000).
48. R. Triolo, V. Bonfante, and F. Lo Celso, private communication (2007); see also N. Kardijlov et al, Neutron tomography in modern archaeology, *Notiziario Neutroni e Luce di Sincrotrone* **13**(2), 6–9 (2008).
49. G. Kühne et al., CNR—the new beamline for cold neutron imaging at the Swiss spallation neutron source SINQ, *Nucl. Instrum. Meth. Phys. Res. A* **542**, 264–270 (2005); ICON: Cold neutron facility for imaging at the Paul Scherrer Institute, Villigen, Switzerland, described in http://neutra.web.psi.ch/facility/index.html.
50. G. Festa for the Ancient Charm collaboration, ANCIENT CHARM: A new project for neutron-based 3D imaging with applications to CH research. Poster Section (Ist prize winner): *Looking Forward to the Past: Science and Heritage*, Tate Modern London (28 November 2006). Available online at http://ancient-charm.neutron-eu.net/ach/conferences.